ORIGINAL RESEARCH PAPER
Volume-9 | Issue-5 | May-2020 | PRINT ISSN No. 2277 - 8179 | DOI : 10.36106/ijsr
INTERNATIONAL JOURNAL OF SCIENTIFIC RESEARCH

STRUCTURAL EXAMINATION OF (PB1-XLAX) TIO3 CERAMICS WITH X-RAY DIFFERECTOMETER

Physics

Pooja Patel Research Scholar, Sankalchand Patel University
Dr.Chirag Patel* Faculty of Science & Humanities, Sankalchand Patel University *Corresponding Author
Dr. Manish Patel Humanities Department, SPCE, Sankalchand Patel University

ABSTRACT

This Paper aims to study various physical properties of La free and lanthanum modified lead titanate ceramic. The Paper starts with the synthesis followed by characterization of the materials. The samples of (Pb1-xLax) Tio3 is synthesized by solid state reaction route and then characterized by XRD techniques. The Rietveld refinement method was employed for structural analysis. The diffused phase transition was analyzed by dielectric measurements.

KEYWORDS

Ceramics, Solid State Reaction Rout, XRD, Structure Analysis

INTRODUCTION

Lead titanate (PbTiO3) is one of the significant ferroelectric resources having perovskite network with excellent dielectric, ferroelectric and electro-optic properties. Physical properties of PbTiO3 (PT) can be considerably customized by substitutions in both the cationic sites by other metal ions with appropriate valence and ionic size. In recent times, a significant interest has been arisen in the area of ferroelectric field due infrared sensors, capacitors, dynamic random access memories (DRAMs) , non-volatile RAMs, un-cooled infrared detectors , piezoelectric actuator, Shutters, optical modulators, microwave, colossal magneto resistance, magneto-electric and electro-optic devices, etc. Crystals of the perovskite family, such as PbTiO3, SrTiO3 and, have been of constant interest because some of these materials show ferroelectric behavior and undergo structural phase transitions [1]. PbTiO3 has been considered to be one of the most important members of this family. It has a high Curie temperature, high pyroelectric coefficient, low dielectric constant, and high spontaneous polarization [2]. Lead titanate (PbTiO3, PT) is a ferroelectric ceramic that has not been proved to be a technologically important material by itself but is a significant component material in electronics such as capacitors, ultrasonic transducers, thermistors, and optoelectronics [3–7]. It is also a promising material for pyroelectric infrared detector applications because of its large pyroelectric coefficient and relatively low permittivity [8, 9]. PbTiO3 (PT) has also been extensively used in a range of piezoelectric applications, as well as being the end member of technologically significant, ferroelectric perovskite series such as PbZr (PZT), Pb(x)Ca(1-x) (PZN-PT), and Pb and so forth. At ambient temperature, the material has a strong anisotropy which develops during cooling through the cubic-tetragonal phase transition of approximately 490°C. The anisotropy as measured by the tetragonality of the unit cell, c/a, may be as high as ~1.06. A large c/a ratio is considered favorable for enhanced electrical properties [10].

SAMPLE PREPERATION

The $Pb_{1-x}La_xTio_3$ (x=0.0,0.10,0.25,0.30 and 0.50) compounds were prepared by conventional solid state route as discussed in chapter 3. The stoichiometric ratio of starting compounds such as lead oxide $(PbO, 99\%)$, lanthanum oxide $(La_2O_3, 99.9\%)$ and titanium oxide $(TiO_2, 99\%)$ were weighed by using a high precision electronic balance. The above compounds were mixed and grinded under acetone using agate mortar and pestle. The grinding was carried out under acetone till the acetone evaporates from the mortar. The mixture was ball milled for 8h to make homogeneous mixture and calcined at 900^0C for 6h. The fine powders of the above samples were pressed into cylindrical pellets of 6 mm diameter and 1 mm thickness under a uni-axial pressure of 6 ton using a hydraulic press. Finally the pellets were sintered at 1100^0C for over 4h with 5% extra lead oxide to compensate the lead loss at high temperature and then cooled to room temperature at the rate of $2^0C\ min^{-1}$. All the above sintering processes were carried out in the air

RESULTS AND DISCUSSION

The XRD patterns of all the samples were recorded by using Philips Analytical Expert-MPD X-ray diffractometer (XRD) (Model- PW3020). The $CuK\alpha$ radiation was used as an X-ray source. The machine was operated at $35kV\ and\ 30mA$. The data were collected with step size of 0.020 and time constant of 1 second. The XRD patterns of $Pb_{1-x}La_xTiO_3$ (PLT) for $x = 0, 0.10, 0.25, 0.30\ and\ 0.50$ calcined at 900^0C for 6 h are shown in Fig. 1. All the samples are in the single phase form. The XRD patterns of $x = 0$ (La free sample) could be indexed to $P4mm$ space group in tetragonal symmetry. However, the La doped samples ($x = 0.10, 0.25, 0.30\ and\ 0.50$) could be indexed using $Pm\bar{3}m$ space group in cubic symmetry. The overlap of the three tetragonal reflections (102), (201) and (210) confirms the tetragonal-to-cubic phase transition. We have not observed any peak corresponds to $P4mm$ space group in the XRD pattern of $x = 0.10$ sample. Hence, it has been found that a phase transition from tetragonal to cubic symmetry with increase of La concentration. Similar behavior has been observed by other research groups on $Pb_{1-x}La_xTiO_3$ materials

CONCLUSIONS

We can say that for 1m^{3}M20 grade of concrete consumption of fine aggregate is 775.96 kg. Here in specimen M-3 we replace fine aggregate by 24.62 kg of crumb rubber for 1m^{3}M20 grades of concrete. So, we can say that up to 15% foundry sand utilized for economical and sustainable development of concrete.Uses of crumb rubberin concrete can reduce the harmfulness to the environment and produce a 'greener' concrete for construction. An innovative supplementary Construction Material is formed through this study.

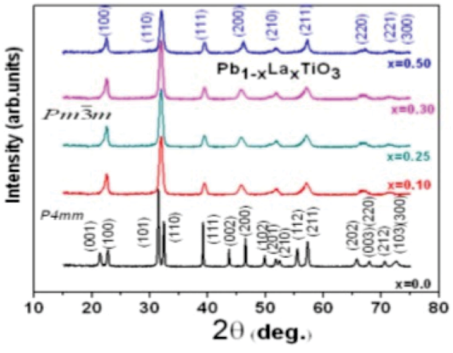

Figure 1: XRD patterns of Pb_(1-x) La_x TiO_3 (PLT) compound for x = 0,0.10,0.25,0.30 and 0.50 calcined at 900°C for 6h.

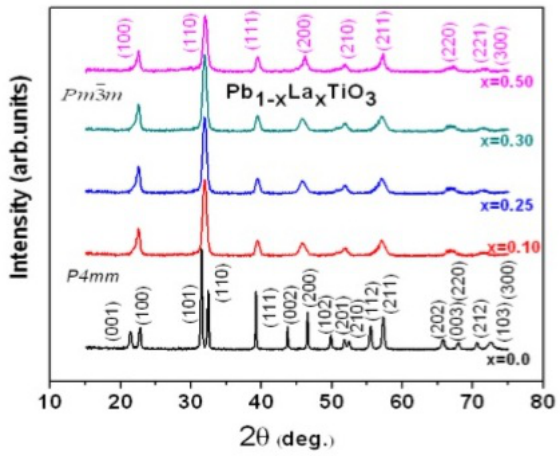

Fig. 2: XRD patterns of Pb_(1-x) La_x TiO_3 (PLT) compound for x = 0,0.10,0.25,0.30 and 0.50 sintered at 1100^0 C for 4h.

The XRD patterns of the samples sintered at 1100^0C for 4h are shown in the Fig. 2. We have observed that, the broadening of XRD peaks has been reduced in 1100^0C sintered samples compare to that of 900^0C calcined samples. We have not observed any additional peak in 1100^0C sintered samples compare to that of 900^0C calcined sample. It reveals that, the structure does not change with the increasing of annealing temperature. However, the crystallite size increases with the increasing of annealing temperature which is discussed in next section. X-ray diffraction is a simpler and easier approach for the determination of crystallite size of powder samples. The underlying principle for such a determination involves precise quantification of the broadening of the diffraction peaks. There are a few techniques involving to calculate the crystallite size such as, Scherrer's method, Williamson- Hall method, and Rietveld refinement method. The Crystallite size obtained from above three different methods (as described in chapter 3) is listed in Table 4.1. We have observed that the crystallite size obtained by Rietveld method is less than that of WH method. It is due to the correction of peak broadening factor taking into account of all instrumental factors. Also the crystallite size obtained by WH method is less than those obtained by Scherrer's formulae. It is because, the strain correction factor has been taken into account in case of WH method whereas it has not taken into account in Scherrer's method. From the above discussion, we conclude that, Rietveld method is the best method among the above three methods to calculate crystallite size for XRD peak broadening. Hence, the crystallite size for all other materials studied in this thesis has been calculated using only Rietveld method. It is observed that crystallite size decreases with increase in La concentration for both the annealed samples. Also the crystallite size increases with increase of sintering temperature for both La free and La substituted samples. The average crystallite sizes (obtained from above three methods) versus La concentration of $Pb_{1-x}La_xTiO_3$, $x = 0.0, 0.10, 0.25, 0.30$ *and* 0.50 samples are shown Fig. 3 (a) and Fig. 3 (b) for the samples calcined at $900^{\circ}C$ and sintered at $1100^{\circ}C$ respectively.

Table 4.1: Average crystallite size (nm) calculated by various methods for the samples $Pb_{1-x}La_xTiO_3$, $x = 0.0, 0.10, 0.25, 0.30$ *and* 0.50 calcined at $900^{\circ}C$ for 6h and sintered at $1100^{\circ}C$ for 4h.

Sample composition	crystallite size (nm)		
	Scherrer's Method	W. H. Method	Rietveld Method
$PbTiO_3$ (900°C)	21.1(5)	16.3(11)	15.9(8)
$PbTiO_3$ (1100°C)	44.2(5)	43.8(3)	43.2(2)
$Pb_{0.90}La_{0.10}TiO_3$ (900°C)	19.8(3)	16.0(3)	15.3(11)
$Pb_{0.90}La_{0.10}TiO_3$ (1100°C)	40.6(12)	40.1(11)	39.1(8)
$Pb_{0.75}La_{0.25}TiO_3$ (900°C)	19.1(10)	15.1(4)	13.4(8)
$Pb_{0.75}La_{0.25}TiO_3$ (1100°C)	38.5(7)	37.8(7)	36.1(2)
$Pb_{0.70}La_{0.30}TiO_3$ (900°C)	17.8(6)	13.8(3)	12.2(9)
$Pb_{0.70}La_{0.30}TiO_3$ (1100°C)	36.6(17)	35.3(13)	34.7(3)
$Pb_{0.50}La_{0.50}TiO_3$ (900°C)	15.4(3)	12.4(5)	11.2(8)
$Pb_{0.50}La_{0.50}TiO_3$ (1100°C)	34.0(4)	30.3(9)	29.3(5)

The XRD patterns were analyzed by employing the Rietveld refinement technique [152] with the help of the FullProf program. In the La free sample ($PbTiO_3$), the T_i, O_1 *and* O_2 are positively shifted along c direction, whereas in the La doped sample (*space group* $Pm\bar{3}m$), these atoms occupy exactly the corners (A site), the face centers (Oxygen's sites), and the body center (B site) of the unit cell, which means the ideal perovskite cubic structure. For all La-containing $PbTiO_3$ samples, the A-site occupancy was shared between *Pb and La*. Considering A-site vacancies only, the refinements of the sample containing unrealistic values for the atomic occupancies and worse statistical compatible parameters, even for the samples with high La content. Nevertheless, it is important to emphasize that realistic occupancy results depend on the atomic number difference between the atoms involved in the site occupancy refinements. In this case, the *Pb* (82) *and La* (57) atomic numbers are significantly different, which usually permits a suitable occupancy refinement.

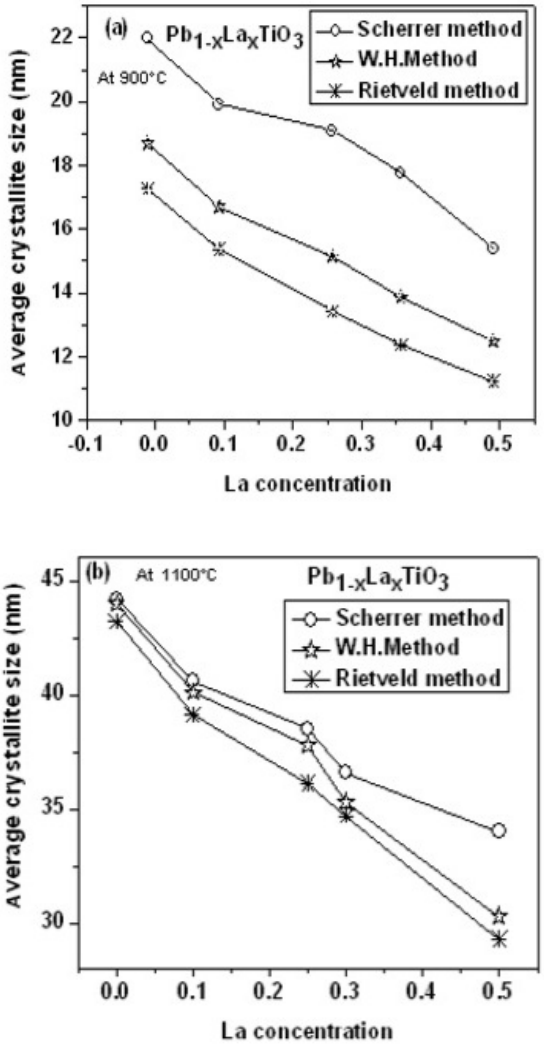

Fig. 3 (a, b): The average crystallite size versus La concentration (a) calcined at 900˚C for 6h and (b) sintered at 1100˚C for 4h of Pb_(1-x) La_x TiO_3 (PLT) powders with (x=0,0.10,0.25,0.30 and 0.50).

The refined XRD patterns of the La free sample (PT) and a typical doped sample $Pb_{1-x}La_xTiO_3$, $x = 0.10$ ($PLT10$) calcined at 900^0C are shown in Fig. 4 and Fig. 5 respectively. Also for La free sample (PT) and a typical doped sample $Pb_{1-x}La_xTiO_3$,$x = 0.10$ (PLT10) calcined at 1100^0C are shown in Fig. 4.6 and Fig. 4.7 respectively. All the observed peaks could be refined using P4mm space group in tetragonal symmetry for La free sample ($PbTiO_3$,$x = 0.00$). However, XRD patterns for La modified samples have been refined using $Pm\bar{3}m$ space group in cubic symmetry.

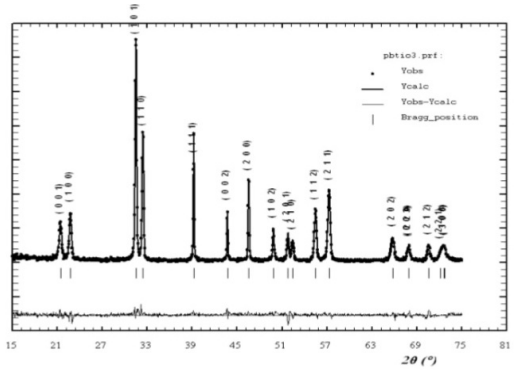

Fig. 4: XRD pattern for $PbTiO_3$ calcined at $900^{\circ}C$ for 6h with refined data obtained by Rietveld method. The experimental points are given as dot (·) and theoretical data are shown as solid lines.

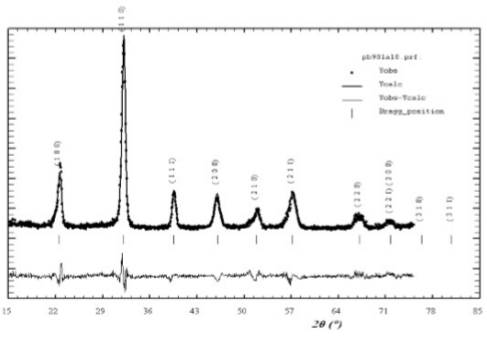

Fig. 5: XRD pattern for the sample $Pb_{0.90}La_{0.10}TiO_3$ calcined at $900^{\circ}C$ for 6h with refined data obtained by the Rietveld method.

The difference between theoretical and experimental data is shown as a bottom line. The vertical lines represent the Bragg's allowed peaks. The experimental points are given as plus (+) and theoretical data are shown as solid lines. The difference between theoretical and experimental data is shown as a bottom line. The vertical lines represent the Bragg's allowed peaks.

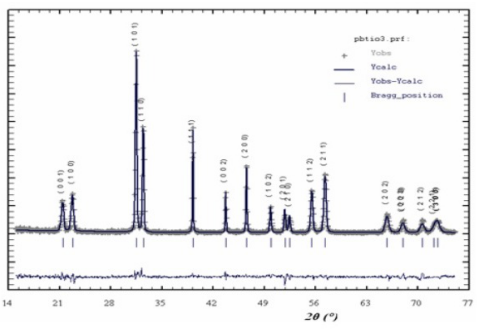

Fig. 6: XRD pattern of $PbTiO_3$ sintered at $1100^{\circ}C$ for 4h with refined data obtained by the Rietveld method.

The experimental points are given as plus (+) and theoretical data are shown as solid lines. The difference between theoretical and experimental data is shown as a bottom line. The vertical lines represent the Bragg's allowed peaks. The experimental points are given as plus (+) and theoretical data are shown as solid lines. The difference between theoretical and experimental data is shown as a bottom line. The vertical lines represent the Bragg's allowed peaks. The Lattice parameters, occupancy, fractional atomic positions etc. were taken as the free parameters during the fitting. The lattice parameters and unit cell volume were found to be decreased with the La concentration; it could be due to the smaller ionic size of La^{3+} (1.06 Å) comparing to that of Pb^{2+} (1.20 Å). The fractional atomic positions and isothermal parameter for 1100^0C sintered sample $PbTiO_3$ *and* $Pb_{0.90}La_{0.10}TiO_3$ ($PLT10$) are shown in Table 2 and Table 3 respectively.

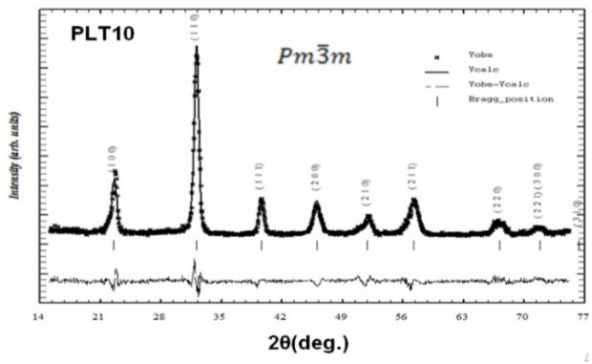

Fig. 7: XRD pattern for $Pb_{0.90}La_{0.10}TiO_3$with refined data obtained by Rietveld method.

The A-site occupancy, lattice parameters, cell volume, the goodness of the fitting parameter is listed in Table 4 and Table 5 for the samples annealed at 900^0C and 1100^0C respectively. The bond lengths and bond angles have been calculated by using the refined parameter with the help of powder cell program. Also we have observed that, the $Pb-Ti, Ti-O_1, Ti-O_2, Pb-O_1$ *and* $Pb-O_2$ bond lengths decreased with the increase in La concentration. The variations of the $Ti-O$ *and* $Pb-O$ distances with lanthanum are shown in Fig. 8 (a) and Fig. 8 (b) for the samples annealed at 900^0C *and* 1100^0C respectively. It has been observed that $Ti-O_2$ *and* $Pb-O_1$ bond lengths remain almost constant for all the samples. This behavior was expected since $Ti-O_2$ *and* $Pb-O_1$ lie on the perpendicular plane to the ferro-distortive axis, which is unaffected by the caxis distortion. On the other hand, it is observed that increasing La content, $Ti-O_1$, *and* $Pb-O_2$ distances are statistically different from La free and La doped samples due to its structural changes and symmetry dependence. The values of bond lengths and bond angles are capitalized for the sample $Pb_{0.90}La_{0.10}TiO_3$ calcined at 900^0C *and* 1100^0C in Table 4 and Table 5 respectively. Using the refined parameters the suggested stable crystal structure of $PbTiO_3$ and $Pb_{0.90}La_{0.10}TiO_3$ are shown in Fig. 9 and Fig. 10 (a-c) respectively.

Table 2: Fractional atomic positions and isothermal parameters of the sample $PbTiO_3$ sintered at $1100^{\circ}C$ for 4h.

Atom	X	Y	Z	Biso
Pb	0.0000	0.0000	0.0000	0.9921
Ti	0.5000	0.5000	0.5377	0.9843
O1	0.5000	0.5000	0.1118	1.0000
O2	0.000	0.5000	0.6174	0.9713

Table 3: Fractional atomic positions and isothermal parameters of the sample $Pb_{0.90}La_{0.10}TiO_3$ sintered at $1100^{\circ}C$ for 4h.

Atom	X	Y	Z	Biso
Pb	0.0000	0.0000	0.0000	0.9921
La	0.0000	0.0000	0.0000	0.9922
Ti	0.0000	0.5000	0.5000	0.9843
O1	0.5000	0.5000	0.0000	1.0000
O2	0.000	0.5000	0.5000	0.9713

Table 4: Parameters obtained from Rietveld analysis of $Pb_{1-x}La_xTiO_3$ (PLT) Powders With (X = 0,0.10, 0.25, 0.30 and 0.50) annealed at $900^{o}C$ for 6 h.

Sample	x=0.0	0.10	0.25	0.30	0.50
Parameter					
Space group	P4mm	$Pm\bar{3}m$	$Pm\bar{3}m$	$Pm\bar{3}m$	$Pm\bar{3}m$
Pb(Occup.)	0.9923(11)	0.8974(8)	0.7415(10)	0.6978(4)	0.4981(2)
La(Occup.)	0.0000	0.1075(1)	0.2494(10)	0.3015(5)	0.5014(2)
Ti(Occup.)	0.9840(7)	0.9840(2)	0.9840(3)	0.9956(7)	0.9840(11)
a = b (Å)	3.9871(8)	3.9602(3)	3.9521(1)	3.9504(6)	3.9324(5)
c (Å)	4.1384(9)	3.9602(3)	3.9521(1)	3.9504(6)	3.9324(5)
Volume (Å^3)	62.9 (2)	62.7 (9)	62.5(3)	62.3(7)	62.2(3)

χ^2 (chi^2)	1.32	2.44	4.62	2.12	4.96
R_p	3.70	19.9	14.7	13.5	12.8
R_{wp}	4.20	24.8	21.3	23.7	18.9
R_{exp}	3.91	8.47	8.59	7.34	6.89
R_{Bragg}	5.63	14.4	4.75	13.7	11.8
R_f	3.21	5.99	3.90	7.09	6.32
Pb-Ti (Å)	3.52(14)	3.48(11)	3.42(21)	3.40(10)	3.38(22)
Ti-O_1 (Å)	2.50(6)	2.46(8)	2.33(7)	2.23(3)	2.05(3)

Table 4.5: Parameters obtained from Rietveld analysis of $Pb_{1-x}La_xTiO_3$ (PLT) powders for $x = 0, 0.10, 0.20, 0.25$ and 0.50 sintered at $1100^{o}C$ for 4 h.

Sample Parameter	x=0.0	0.10	0.25	0.30	0.50
Space group	P4mm	$Pm\bar{3}m$	$Pm\bar{3}m$	$Pm\bar{3}m$	$Pm\bar{3}m$
Pb(Occup.)	0.9976(17)	0.8874(12)	0.7315(11)	0.6878(1)	0.4981(12)
La(Occup.)	0.0000	0.1095(11)	0.2324(10)	0.3040(4)	0.5084(7)
Ti(Occup.)	0.9965(22)	0.9720(2)	0.9720(2)	0.9956(7)	0.9720(2)
a = b (Å)	3.9887(3)	3.9402(8)	3.9385(11)	3.9383(7)	3.9321(5)
c (Å)	4.1380(9)	3.9402(8)	3.9385(11)	3.9383(7)	3.9321(5)
Volume (Å^3)	62.8(2)	62.1(4)	61.8(13)	61.1(3)	60.2(4)
χ^2 (chi^2)	2.04	4.53	4.53	3.62	2.37
R_p	18.7	22.1	22.1	19.9	18.4
R_{wp}	24.8	28.8	20.6	21.8	24.1
R_{exp}	12.2	12.4	10.4	9.56	15.6
R_{Bragg}	13.3	12.4	11.4	12.7	12.4
R_f	8.2	10.1	5.1	8.52	7.7
Pb-Ti (Å)	3.55(14)	3.47(11)	3.45(11)	3.41(14)	3.39(2)
Ti-O_1 (Å)	2.55(7)	2.53(3)	2.51(9)	2.48(6)	2.45(7)
Ti-O_2 (Å)	2.18(5)	2.17(6)	2.15(7)	2.14(9)	2.12(5)
Pb-O_1 (Å)	3.41(5)	3.40(2)	3.38(8)	3.36(8)	3.34(3)
Pb-O_2 (Å)	4.58(3)	4.47(7)	4.43(6)	3.96(4)	3.85(7)
∠Pb-Ti-O_1	71.96(2)	102.13(1)	102.73(1)	102.73(1)	102.73(1)
∠Pb-Ti-O_2	84.01(2)	145.55(2)	145.55(2)	145.55(2)	145.55(2)
∠Pb-Ti-Pb	77.19(3)	71.52(4)	71.52(4)	71.52(3)	71.52(4)
∠O_2-Ti-O_2	107.14(6)	149.11(3)	149.11(3)	149.11(2)	149.11(1)

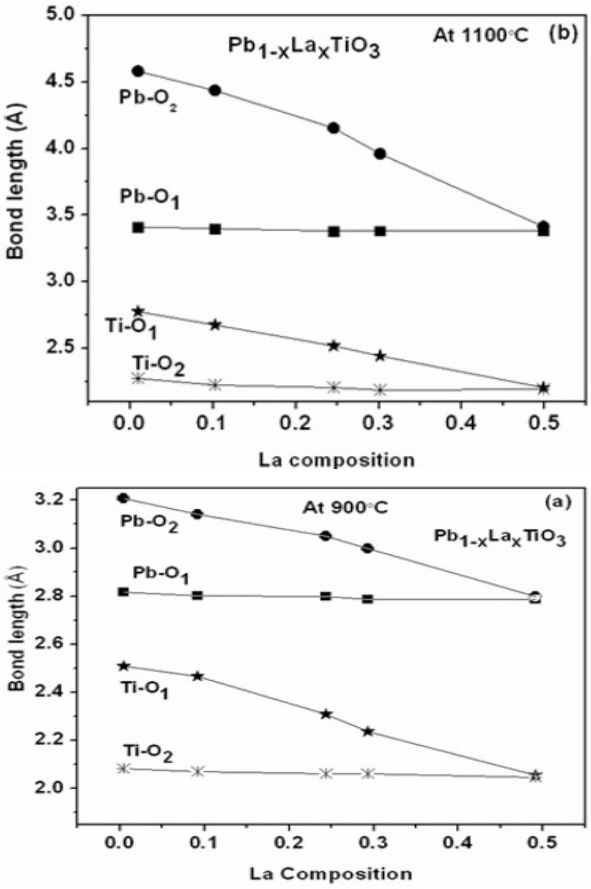

Fig. 8 (a, b): The dependence of the $Ti-O$ and $Pb-O$ bond lengths with the La content of $Pb_{1-x}La_xTiO_3$ samples of $x = 0, 0.10, 0.25, 0.30$ and 0.50 (a) calcined at $900^{\circ}C$ for 6 h and (b) sintered at $1100^{\circ}C$ for 4h.

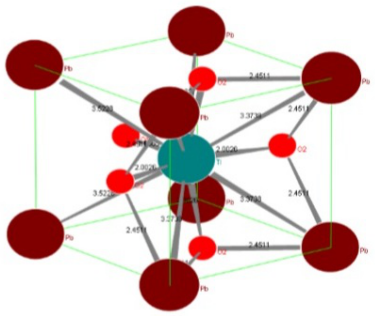

Fig. 9: Structure of obtained from the Rietveld analysis parameters

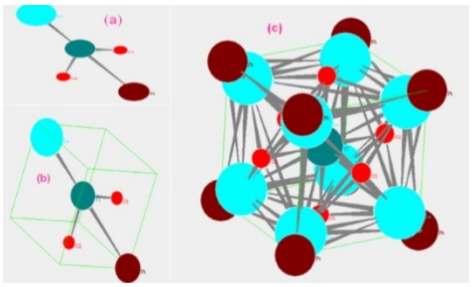

Fig. 10 (a-c): (a) Positions of the atoms, (b) position of the atoms in crystal co-ordinate and (c) crystal structure of a typical sample obtained from the Rietveld analysis parameters

REFERENCES:

[1]. F. Jona and G. Shirane, Ferroelectric Crystals, MacMillan, New Yor k, NY, US A, 1962 .
[2]. R. Migoni, H. Bilz, and D. Bauerle, "Origin of raman scattering and ferroelectricity in oxidic perovskites," Physical Review Letters, vol. 37, no. 17, pp. 1155–1158, 1976.
[3]. L. E. Cross, "Dielectric, piezoelectric and ferroelectric components," The Bulletin of the American Ceramic Society,vol.63, pp. 586–590, 1984.
[4]. K. Sasazawa, K. Oshima, and N. Yamaoka, "Surface potential decay and residual voltage measurements in highly elongated polyethylene," Japanese Journal of Applied Physics,vol.26, pp. L65–L67, 1987.
[5]. T. R. Shrout and A. Halliyal, "Preparation of lead-based ferroelectric relaxors for capacitors," American Ceramic Society Bulletin,vol.66,pp.704–711,1987.
[6]. D. Damjanovic, T. R. Gururaja, and L. E. Cross, "Anisotropy in piezoelectric properties of modified lead titanate ceramics," American Ceramic Society Bulletin,vol.66, no.4,pp.699–703, 1987.
[7]. M. Kuwabara, "Lead titanate ceramics with positive temperature coefficients of resistivity," Journal of the American Ceramic Society,vol.73,no.5, pp.1438–1439,1990.
[8]. Y. Chan, H. L. W. Chan, and C. L. Choy, "Nanocrystalline lead titanate and lead titanate/vinylidene fluoride-trifluoroethylene 0-3 nanocomposites," Journal of the American Ceramic Society, vol. 81, no. 5, p. 1231, 1998.
[9]. R. Y. Ting, "Evaluation of new piezoelectric composite materials for hydrophone applications," Ferroelectrics, vol.67,no. 1,pp. 143–157, 1978.
[10]. G. Shirane and S. Hoshino, "On the phase transition in lead titanate," JournalofthePhysicalSocietyofJapan,vol.6, pp.265– 270, 1951.